GEOLOGICA CARPATHICA, AUGUST 2010, 61, 4, 327–339 doi: 10.2478/v10096-010-0019-y

Post-magmatic hydrothermal mineralization associated with Cretaceous picrite (Outer Western Carpathians, Czech Republic): interaction between host rock and externally derived fluid

ZDENĚK DOLNÍČEK✉, TOMÁŠ URUBEK and KAMIL KROPÁČ

Department of Geology, Palacký University, Tř. 17. listopadu 12, 771 46 Olomouc, Czech Republic; ✉dolnicek@prfnw.upol.cz

(Manuscript received November 20, 2009; accepted in revised form March 11, 2010)

Abstract: Mineralogy, fluid inclusions, C, O, S, Sr isotopes and trace elements have been studied in amygdule and vein mineralization hosted by the Lower Cretaceous effusive picrite at Hončova hůrka (Silesian Unit, Flysch Belt of the Outer Western Carpathians). Besides dominating dolomite, magnesite, siderite, quartz, calcite, chlorite, glauconite, fluorite, barite, pyrite and millerite were also identified. The parent fluids are characterized by low temperatures (< 50–170 °C), low salinities (0.4 to 3.7 wt. % NaCl eq.), low content of strong REE-complexing ligands, $\delta^{18}O$, $\delta^{13}C$ and $\delta^{34}S$ ranges of 0/+ 14 ‰ SMOW, 0/–9 ‰ PDB and ~0 ‰ CDT, respectively, and initial $^{87}Sr/^{86}Sr$ ratios much more radiogenic (0.7060 to 0.7068) than those of host picrite (0.7042 and 0.7046). The fluids are interpreted to be predominantly of external origin, derived from mixing of seawater with diagenetic waters produced by dewatering of clay minerals in the associated flysch sediments. The isotope and REE signatures indicate interaction of at least a part of fluids with sedimentary carbonates. The interaction of fluids with host picrite led to strong alteration of rock-forming minerals and leaching of some elements (Mg, Ni, S, partly also REE) that widely participated during precipitation of vein- and amygdule-hosted mineral phases.

Key words: Outer Western Carpathians, stable isotopes, strontium isotopes, fluid-rock interaction, veins, fluid inclusions, amygdules, REE, picrite.

Introduction

The mafic and alkaline-to-subalkaline igneous rocks of the teschenite association are widespread in the area between Hranice in the Czech Republic and Bialsko-Biała in Poland, which belongs to the Silesian Unit of the Outer Western Carpathians (Fig. 1). The magmatic rocks forming sills, dikes, submarine extrusions and pillow lavas are classified as teschenites, picrites, monchiquites and alkaline basalts (Pacák 1926; Smulikowski 1929; Kudělásková 1987; Hovorka & Spišiak 1988). Although these rocks were the subject of long-lasting scientific interest (the term "teschenite" was defined precisely in this area in the second half of the 19th century), many aspects of their origin remain unresolved.

A typical feature of these rocks is the intense hydrothermal alteration, characterized by pervasive chloritization, serpentinization, carbonatization, silicification and zeolitization of primary magmatic mineral phases (Pacák 1926; Šmíd 1962; Trundová 2004). Besides the alteration of rock-forming minerals, also amygdule fill and mineral veins developed in magmatic rocks at many sites. The hydrothermal assemblages are formed mainly by carbonates, chlorite, quartz, opal or chalcedony, locally also zeolites and/or sulphides occur (Bernard et al. 1981; Sušeň 2000; Urubek 2009). The source of mineralizing fluids is still under debate. Considering the geological position of the magmatic suite, the earlier researchers (Pacák 1926; Šmíd 1962) proposed seawater as the main source of fluids (cf. also Kiss et al. 2008), which can be possibly combined with magmatic waters remaining after crystallization of host igneous rocks. However, the hypothesis has not been supported by relevant data. Recently, Dolníček et al. (2010) showed that magmatic fluids were responsible only for early mineralization of titanite, aegirine-augite, annite, strontian apatite and analcime, whereas the younger assemblage of carbonates, chlorite, quartz and sulphides precipitated from an externally derived fluid supplied by the surrounding sedimentary sequences.

In this contribution we characterize mineralogically and genetically the hydrothermal mineralization from well-known mineralogical site at Hončova hůrka Hill. The mineralogical study extends early descriptive papers by Rusek & Valošek (1968) and Kudělásková et al. (1990). Furthermore, our study is supplemented by trace element, fluid inclusion, and C, O, S and Sr isotope data enabling a more complex evaluation of the origin of the mineralization.

Geological setting

The study area is situated in the Outer Western Carpathians, an external part of the Alpine-type orogenic belt of the Western Carpathians (Plašienka et al. 1997). The Externides consist of Middle-to-Upper Miocene Molasse Basin of the Carpathian Foredeep, and Upper Jurassic-to-Early Miocene fold-and-thrust Flysch Belt, representing the Tertiary accretionary wedge of the Carpathian orogen. In the NE part of the Czech Republic, the Flysch Belt is subdivided into the Subsilesian, Silesian and Magura Nappes, listed from tectonic

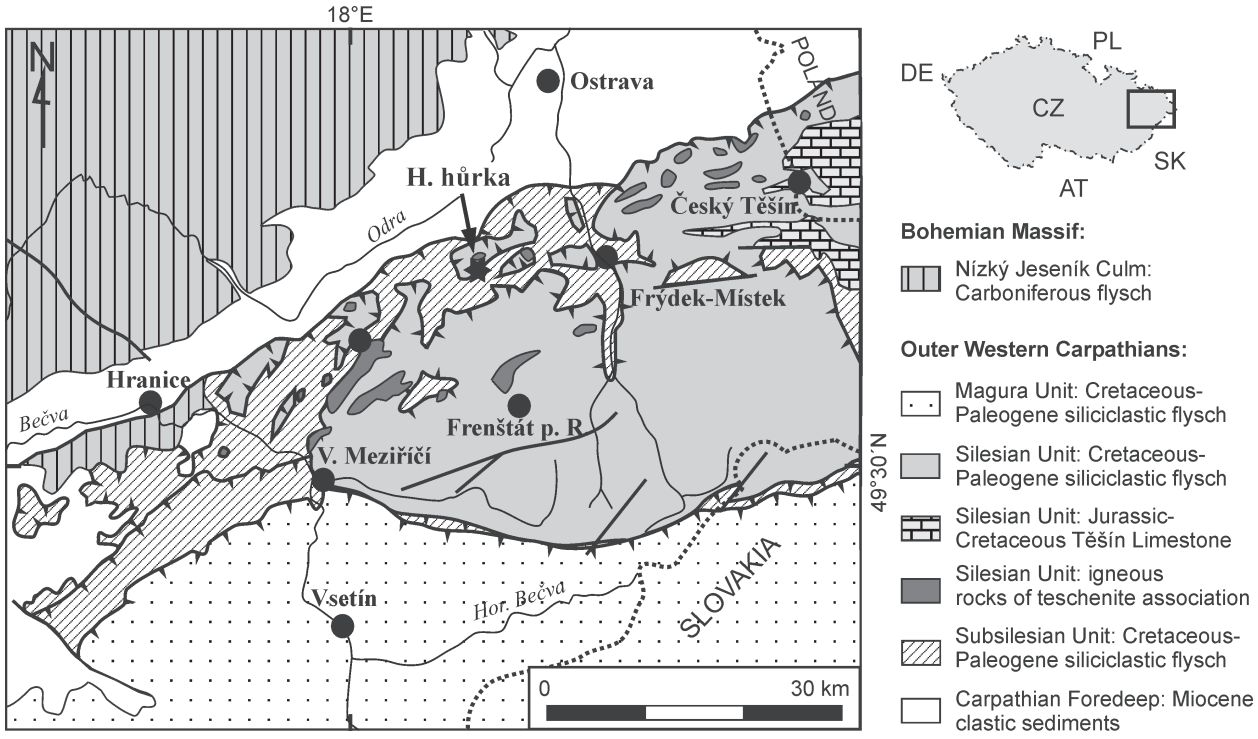

Fig. 1. Geological position of the Hončova hůrka locality in the Outer Western Carpathian's flysch nappe system.

foot-wall to hanging-wall (Fig. 1). The studied locality is situated in the Silesian Unit consisting mainly of Upper Jurassic-to-Upper Oligocene marine sediments (Eliáš 1970). The basal carbonate-rich rocks (Těšín Limestone of the Late Jurassic-Early Cretaceous age) are followed by rhythmic and cyclic flysch sedimentation of claystones, sandstones, and rare conglomerates of Early Cretaceous to Late Oligocene age. Locally, siderite horizons are present in claystone-rich cycles (e.g. Hradiště Formation, Veřovice Formation), layers of dark organic-rich biogenic silicite (Menilite Formation) and bodies of teschenite rocks association (Hradiště Formation). The whole-rock sequence was folded and thrusted towards the NW (over the SE part of the Bohemian Massif, Fig. 1) during the Alpine Orogeny in Paleocene–Miocene times.

Based on the field and geochronological evidence (Lucińska-Anczkiewicz et al. 2002; Grabowski et al. 2003), the intrusion of the teschenite rock association was coeval with sedimentation of the Lower Cretaceous Hradiště Formation. The mostly mafic quartz-free alkaline-to-subalkaline rocks are very variable in texture, mineral composition and chemistry, which is interpreted as a result of fractional crystallization, mixing of magmas of different origins, assimilation of sedimentary rocks and post-magmatic alterations (Kudělásková 1987; Hovorka & Spišiak 1988; Dostal & Owen 1998; Wlodyka & Karwowski 2004). In general, the most primitive rocks are picrites, and the most evolved and fractionated are teschenites. The rocks have high concentrations of incompatible elements (Ti, P, Zr, LREE) and low contents of compatible trace elements (Cr, V). The interpretation of their geotectonic setting is not conclusive. Narębski (1990) and Spišiak & Hovorka (1997) stated their geochemical affinity to within-plate basalts generated during the early rifting in the Silesian Unit. By contrast, Dostal & Owen (1998) interpreted these rocks ("lamprophyres") as post-tectonic intrusions bound to reactivation of deep faults during the Early Cretaceous.

The studied locality (N49° 39.575′, E18° 09.176′, altitude 317 m a.s.l.) is an old quarry situated 2 km north of the town of Příbor on the western slope of the Hončova hůrka Hill. The quarry is situated in a nappe relic of the Silesian Unit, which overlies the Subsilesian Unit. A dominating part of the quarry is formed by black-green effusive rocks belonging to peridotite picrite, which often exhibits the porphyric and/or amygdaloid texture (Kudělásková 1987; Matýsek 1989). The contact with clastic sediments (dark claystones with interpositions of sandy limestones) of the Hradiště Formation is exposed in the S and SE wall, where thermal metamorphism gave rise to grey calcareous contact hornfels. Throughout the whole quarry, the picrite is strongly altered. Phenocrysts of primary mafic minerals, olivine, clinopyroxene, biotite as well as the groundmass (taking 25–36, 13–44, 1–6, and 16–35 vol. %, respectively; Kudělásková 1987) are partly or completely changed into a mixture of chlorite, serpentine and carbonate. Chemical compositions of three rock samples that differ in degree of alteration are given in Table 1. The hydration and carbonatization effects are marked by increased loss on ignition (up to 17 wt. %), calcium (up to 12 wt. % CaO) and CO_2 (up to 7.8 wt. %). By contrast, the contents of magnesium and iron are depleted in altered samples.

Both the picrite and sediments are cut by white to pinkish hydrothermal veinlets <1 to 30 mm thick and up to several meters long. Laterally, the thickness is quite constant for individual veins. A NW-SE striking system of steep (55–85°) veinlets has been recognized. The tectonic striae have never been observed in the vein fill nor on the contact of the rock

Table 1: Chemical composition of selected samples from Hončova hůrka. Analysis No. 44 is taken from Kudělásková (1987). LOI — loss on ignition, F/FM — FeO/(FeO+MgO) weight ratio, n.d. — not determined.

Sample	HH-4 Picrite	44 Picrite	HH-1 Picrite	HH-3 Dol. II+magn
P_2O_5	0.41	0.65	0.81	0.03
SiO_2	39.09	37.10	35.58	0.75
TiO_2	1.87	2.15	2.66	<0.01
Al_2O_3	8.00	11.60	10.61	<0.01
Cr_2O_3	0.13	n.d.	0.11	0.02
FeO^{tot}	11.25	10.08	7.12	5.60
MnO	0.16	0.18	0.11	0.04
MgO	21.00	17.20	9.45	24.55
CaO	8.87	12.20	12.39	19.50
Na_2O	1.35	0.75	0.30	0.04
K_2O	0.99	0.55	1.86	<0.01
LOI	5.00	6.50	17.70	46.70
Total	97.70	98.96	97.88	97.20
CO_2	1.28	4.28	7.81	49.03
S^{tot}	0.07	n.d.	0.02	<0.02
F/FM	0.35	0.37	0.43	0.19

and vein. There are no open drusy cavities, all fissures are completely cemented. Brecciation of the host rocks has sometimes been observed.

Methods

The electron microprobe analyses of minerals were performed using a Cameca SX-100 microprobe at the Masaryk University in Brno. For carbonate and silicate minerals, the acceleration voltage of 15 kV, 20 nA beam current and beam diameter of 10 μm (carbonates) and 5 μm (phyllosilicates), respectively, were used. For sulphide minerals, voltage of 25 kV, beam current of 20 nA and beam diameter of 1 μm were applied. The collected data were converted to wt. % using the automatic PAP procedure (Pouchou & Pichoir 1985). Synthetic phases and well-defined minerals have been used as standards.

Fluid inclusions were investigated by means of petrography and optical microthermometry in standard doubly polished wafers and cleavage fragments. Primary (P), primary-secondary (PS) and secondary (S) inclusions were distinguished according to the criteria given by Roedder (1984) and Shepherd et al. (1985). Microthermometric parameters were measured using a Linkam THMSG 600 stage at Palacký University, Olomouc. The temperature of final homogenization (T_h), eutectic temperature (T_e) and melting temperature of ice ($T_m$ice) were measured. The stage was calibrated with inorganic standards and synthetic fluid inclusions. The reproducibility is within 0.1 °C for temperatures between −56.6 and 0 °C, and within 1 °C at 374.1 °C.

For bulk chemical analyses, the carbonate samples weighing between 1 and 2 g were hand-picked under a binocular microscope and then pulverized in an agate mortar. The host rock was powdered in an epicyclic mill and reduced in weight by quartering. Chemical analyses were performed in the ACME Analytical Laboratories, Vancouver, Canada. Aliquots for heavy metal analyses were dissolved in hot (95 °C) aqua regia and analysed using the ICP-ES method. Other determined elements including refractory metals and rare earth elements (REE) were analysed by ICP-MS in another sample aliquot decomposed using $LiBO_2$ fusion followed by leaching in diluted (5%) HNO_3. Reproducibility of results is within 5–10 % based on repeated analyses. The Ce and Eu anomalies were calculated using the equations given by McLennan (1989).

Stable isotope analyses were conducted in the laboratories of the Czech Geological Survey, Prague, using a Finnigan MAT 251 mass spectrometer. The conversion of carbonates to CO_2 was made by reaction with 100% orthophosphoric acid (McCrea 1950). For sulphur isotope analyses, the samples were firstly decarbonatized using 10% HCl. Sulphidic sulphur in the insoluble residuum was converted to sulphate using HNO_3-HCl mixture (Jarchovský 1960), and precipitated as barium sulphate. The SO_2 gas for sulphur isotope analysis was produced by heating of $BaSO_4$ with a $SiO_2+V_2O_5$ mixture (Ueda & Krouse 1987) at 1050 °C. Results of isotope analyses are conventionally expressed in delta (δ) notation as per mil (‰) deviation from commonly used standards (PDB, SMOW, CDT). Uncertainty is better than ±0.05, ±0.1, and ±0.2 ‰ for C, O and S isotopic composition, respectively. The isotopic composition of the parent fluid was calculated using the equations published by O'Neil et al. (1969) and Ohmoto & Goldhaber (1997). When calculating the fluid $\delta^{13}C$ value, equations for H_2CO_3 and HCO_3^- as dominating carbon species were used for temperatures above and below ~120 °C (cf. Matsuhisa et al. 1985), respectively.

For strontium isotope determinations, the splits of powdered samples used for trace element determinations were decomposed using HCl (carbonates) or HNO_3-HCl-HF mixture (rocks). Strontium was isolated on PP columns with Sr.spec Eichrom resin. The Sr isotopic ratios were measured using a Finnigan MAT 262 thermal ionization mass spectrometer in dynamic mode using a double Re filament assembly in the isotope laboratory of the Czech Geological Survey, Prague. The $^{87}Sr/^{86}Sr$ ratios were corrected for mass fractionation to $^{86}Sr/^{88}Sr=0.1194$. External reproducibility was controlled by repeated analyses of the NBS 987 ($^{87}Sr/^{86}Sr=0.710247$ ±26 (2σ), n=25) isotopic standard. The decay constant of $1.42*10^{-11}$ yr^{-1} was used for subsequent calculations (Steiger & Jäger 1977).

Results

Mineralogy

Veins

The mineral composition of all veins is very simple, they are formed only by carbonates. We have not recently observed zeolite minerals (harmotome, heulandite, ferrierite) described by Kudělásková et al. (1990). The claystone-hosted veins are filled by white coarse-crystalline calcite (isometric grains up to 1 cm in size; sample HH-7). By contrast, the picrite-hosted ~0.5 cm thick veinlets are formed by white to pinkish fibrous dolomite, with individual fibres arranged

perpendicular to the walls of the vein (sample HH-5). No remnants of host picrite occur within the vein. The WDX analyses proved chemical homogeneity of the carbonate containing ~91, ~8.5 and ~0.5 mol % of dolomite, ankerite and kutnohorite, respectively.

Amygdules

The amygdules are distributed highly irregularly in the host picrite: in some parts they are missing, in foamed portions of rock the total volume of amygdules is much higher than those of rock-forming picrite matrix. The sizes are variable, ranging from <1 mm up to 1 m (Rusek & Valošek 1968). The amygdules often display zonal texture and highly variable mineral composition precluding the construction of an unified paragenetic sequence. Rusek & Valošek (1968) described dolomite, ankerite, calcite, quartz, chalcedony, opal, hematite, barite, celadonite, chlorite, goethite, rutile, and pyrite in the amygdule fill. Recently, we have studied in a greater detail three samples that differ in size, texture and mineral composition.

1) Sample HH-1 consists of foamed picrite containing ~80 vol. % of white to pinkish spherical amygdules reaching 2–4 mm in diameter. All the amygdules are completely filled up by minerals and often exhibit a zonal structure (Fig. 2a). The dominating constituent is dolomite showing an oscillatory growth zonality in BSE image (Fig. 2a). It contains 92–96, 3.7–7.5 and ~0.3 mol % of dolomite, ankerite and kutnohorite molecules, respectively. Growth zonality of dolomite is highlighted by tiny interpositions or inclusions of calcite ($Cal_{93-98}Mag_{0.7-4.3}Sid_{0.1-1.8}Rdc_{0.3-0.5}Str_{0.1-0.3}$). The youngest central part of the amygdule is filled by either quartz (sample HH-1) or calcite (sample HH-17).

2) Sample HH-2 is a potato-shaped amygdule 1.5 cm in diameter, with concentric zonal texture. The oldest part is formed by pink-grey hemispherical aggregates of dolomite with a spherulitic arrangement of strongly elongated dolomite individuals. Compositional zonality has not been proved using the microprobe ($Dol_{94.2-94.6}Ank_{5.4-5.7}Ktn_{0.2-0.4}$). Dolomite aggregates are rimmed by dark brown 0.5–1 mm thick layers of calcite I ($Cal_{97.8}Mag_{1.2}Sid_{0.4}Rdc_{0.4}Str_{0.2}$), which are followed by coarse-grained (up to 5 mm) rhombohedral crystals of colourless to white quartz. In the central vug, white to colourless rhombohedral crystals of calcite II are present.

3) Sample HH-3 represents the largest (~15 cm in size) and mineralogically most interesting amygdule (Fig. 2b). Macroscopically, three distinct types of fill can be distinguished. The oldest marginal part adjacent to the host rock is composed of white to grey-pink middle-grained (0.5–1 mm) dolomite I. The individual isometric crystals often show colour zonation (milky white cores rich in fluid inclusions and transparent rims much poorer in fluid inclusions). Microprobe analyses showed a limited chemical variability (93–98 mol % dolomite, 1.4–6.8 mol % ankerite, 0.2–0.6 mol % kutnohorite). The growth zonality of the dolomite I is highlighted by 2–3 interpositions rich in irregularly shaped patches (Fig. 2e) of a fine-grained green phyllosilicate, essentially isotropic under crossed polars. The mineral resembles celadonite suggested by Rusek & Valošek (1968), however, with respect to its chemical composition (Table 2) showing generally low contents of interlayer cations (0.61–0.75 apfu K+Na+Ba+Ca) it is classified as glauconite according to Rieder et al. (1997) — Fig. 3c. Weathered glauconite becomes brown in thin section and loses potassium (analyse No. 6 in Table 2).

The central part of the amygdule is completely filled by a massive fine-grained carbonate whose colour is white-to-pink in fresh parts and brown in partly weathered parts. Moreover, this material also fills sporadic fissures within marginal dolomite I (Fig. 2b). In thin section, a mosaic of the very fine-grained (5–10 μm) poorly transparent isometric carbonate grains is observed. In BSE image, two spatially distributed mineral phases can be distinguished. The major lighter phase is dolomite II ($Dol_{86.4-88.9}Ank_{11.0-13.5}Ktn_{0.0-0.1}$), whereas the minor darker one is magnesite ($Mag_{87.5-88.6}Sid_{10.1-11.2}Cal_{1.0-1.2}Rdc_{0.0-0.1}$). The bulk chemical composition of this carbonate mixture is given in Table 1. Based on Mg and Ca balance, the central part of amygdule is composed of 72 and 28 (±2) wt. % of dolomite II and magnesite, respectively.

Spherical ball-like aggregates of greenish carbonate occur locally in between the marginal dolomite I zone and central fine-grained carbonate. Sometimes they are concentrated immediately along the contact, sometimes they are freely "swimming" in the fine-grained dolomite-magnesite matrix (Fig. 2b). Each aggregate exhibits a distinct growth zonality, visible in both optical and electron microscopes (Fig. 2c). The crystallization started usually by compositionally homogeneous euhedral lenticular crystal of dolomite with lowermost content of iron ($Dol_{96.8}Ank_{3.1}Ktn_{0.1}$). An irregular grain of barite was observed exceptionally in the centre of this dolomite crystal. The most voluminous remnants of the aggregate are constituted by well-elongated individuals of carbonate oriented perpendicular to the surfaces of early dolomite crystals. The carbonate is mostly iron-richer dolomite III ($Ank_{3.3-7.0}Ktn_{0.0-0.6}$), which contains tiny (up to 80 μm thick) interpositions (Fig. 2c) or layers of discrete inclusions of Mg-Fe-rich carbonate ($Mag_{38-48}Sid_{38-44}Cal_{13-18}Rdc_{0.4-0.5}$). The carbonate exhibits a detailed growth zonality (Fig. 2d), with composition lying just around the border between Mg-siderite and Fe-magnesite in the classification scheme of Trdlička & Hoffman (1975) — Fig. 3a. The greenish colour of the dolomite III is caused by spatially distributed minute worm-like, fan-like or irregular aggregates of chlorite. This mineral also occurs in the interspace matrix within clusters of the described ball-like dolomite aggregates (Fig. 2f). WDX analyses proved trioctahedral Fe-Mg chlorites (Table 2). High Si contents (3.25–3.94 apfu) and variable Fe/(Fe+Mg) ratios (0.49–0.66) correspond to delessite to pennine (Melka 1965) — Fig. 3b. Finally, both the ball-like dolomite aggregates and their interspace matrix contain rare sulphide grains, represented by up to 60 μm large spherical grains of older pyrite and up to 250 μm long needles of younger millerite (Fig. 2f). Pyrite contains elevated contents of Ni (1.3–1.9 wt. %), Co (0.2–0.4 wt. %) and Cd (0.15–0.18 wt. %), millerite contains increased Fe (0.9–2.0 wt. %) and Co (0.2–0.5 wt. %). The contents of Ag, Zn, As, Se, In and Mn are below the detection limits of the microprobe.

Fluorite was rarely found to occur as irregular coarse-grained aggregate at the contact of picrite and central fine-

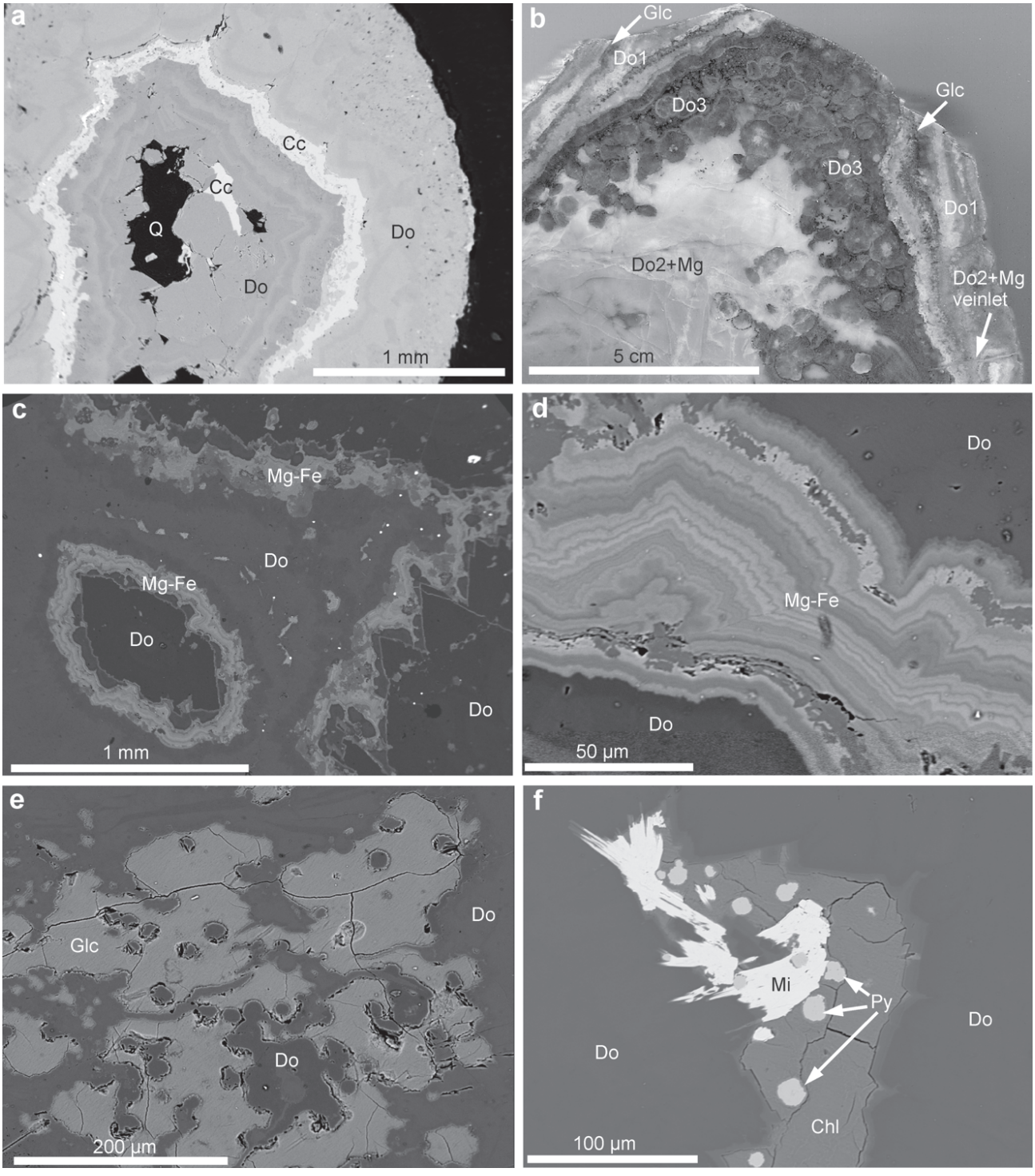

Fig. 2. Textural features and mineral paragenesis of hydrothermal mineralization from Hončova hůrka. **a** — Compositionally zonal fill of an amygdule hosted by sample HH-1. Do — dolomite, Cc — calcite, Q — quartz. BSE image. **b** — Three populations of carbonate hosted by amygdule HH-3. Early dolomite I (Do1) contains interpositions formed by glauconite (Glc) and is cut by a tiny veinlet composed of dolomite II+magnesite (Do2+Mg) filling also the central part of the amygdule. The spherical aggregates of dolomite III (Do3) are distributed mainly along the contact of both above mentioned phases. **c** — Growth zonality of carbonates. The crystallization of dolomite III (Do) was broken by interposition of Fe-rich magnesite to Mg-rich siderite (Mg–Fe). The white dots are small pyrite grains. Sample HH-3, BSE image. **d** — Detailed growth zonality of Fe-rich magnesite to Mg-rich siderite (Mg–Fe) from figure c. **e** — Irregular aggregates of glauconite (Glc) enclosed within dolomite I (Do). Sample HH-3, BSE image. **f** — Fine-grained aggregate of chlorite (Chl) enclosed in dolomite III (Do) contains rounded pyrite grains (Py) which are overgrown by millerite (Mi). Sample HH-3, BSE image. All BSE images were made by M. Dosbaba and P. Gadas.

Table 2: Representative microprobe analyses of vein glauconite (anal. No. 1–5 fresh glauconites, No. 6 weathered one) and chlorite (anal. No. 7–10) from Hončova hůrka. The empirical formulae have been calculated for 11 and 14 anions per formula unit for glauconite and chlorite, respectively.

	1	2	3	4	5	6	7	8	9	10
P_2O_5	0.06	0.08	0.02	0.05	n.d.	0.22	0.19	0.27	0.19	0.04
SiO_2	49.68	50.18	52.30	51.31	53.27	50.68	37.07	36.66	37.53	31.37
TiO_2	0.01	0.00	0.01	0.02	0.02	0.00	0.07	0.06	0.06	0.00
Al_2O_3	8.26	8.12	9.25	9.43	7.84	12.37	9.13	9.73	9.59	14.50
Cr_2O_3	0.00	0.01	0.00	0.00	0.00	0.03	0.02	0.00	0.02	0.04
FeO^{tot}	18.66	19.32	17.61	17.84	18.29	6.87	31.14	32.11	31.68	27.15
MgO	4.58	4.83	4.71	4.55	7.86	15.07	9.42	9.27	9.53	14.83
MnO	0.00	0.02	0.00	0.02	0.03	0.05	0.02	0.00	0.02	0.02
CaO	0.51	0.56	0.75	0.55	0.53	1.21	1.63	1.26	1.06	0.74
BaO	0.00	0.01	0.00	0.02	n.d.	0.03	0.00	0.05	0.00	0.01
NiO	0.07	0.06	0.02	0.08	n.d.	0.08	n.d.	n.d.	n.d.	0.19
ZnO	0.02	0.04	0.00	0.00	0.01	0.02	0.00	0.04	0.04	0.07
Na_2O	0.04	0.07	0.03	0.06	0.08	0.30	0.10	0.08	0.08	0.03
K_2O	7.46	7.09	7.19	7.14	6.35	0.96	0.17	0.14	0.13	0.01
Cl	0.04	0.04	0.04	0.05	0.03	0.09	0.02	0.01	0.00	0.02
F	0.00	0.00	0.00	0.00	0.00	0.00	0.00	0.00	0.00	0.00
Total	89.40	90.43	91.92	91.12	94.30	87.75	88.97	89.69	89.94	89.01
P	0.004	0.005	0.001	0.003		0.013	0.017	0.024	0.017	0.004
Si	3.648	3.640	3.698	3.667	3.666	3.546	3.906	3.846	3.904	3.268
Ti	0.001			0.001	0.001		0.005	0.005	0.004	
Al	0.715	0.695	0.771	0.794	0.636	1.020	1.134	1.203	1.176	1.780
Cr		0.001				0.002	0.002		0.002	0.003
Fe^{3+}	1.146	1.172	1.041	1.066	1.053	0.402				
Fe^{2+}							2.744	2.817	2.756	2.366
Mg	0.501	0.522	0.497	0.485	0.806	1.572	1.479	1.450	1.478	2.304
Mn		0.001		0.001	0.002	0.003	0.001		0.002	0.002
Ca	0.040	0.043	0.057	0.042	0.039	0.091	0.184	0.141	0.118	0.082
Ba				0.001		0.001		0.002		
Ni	0.004	0.003	0.001	0.005		0.005				0.016
Zn	0.001	0.002				0.001		0.003	0.003	0.005
Na	0.006	0.010	0.004	0.008	0.010	0.041	0.020	0.017	0.016	0.005
K	0.699	0.656	0.649	0.651	0.558	0.085	0.022	0.019	0.017	0.001
Cl	0.005	0.005	0.005	0.006	0.004	0.011	0.003	0.002		0.004
Catsum	6.765	6.749	6.718	6.724	6.771	6.781	9.515	9.528	9.493	9.836

Table 3: Results of fluid inclusion microthermometry. Temperature parameters are in °C, salinity in wt. % NaCl eq.

Sample	Sample type	Mineral	FI type	Phase composition	T_h (L+V)	T_f	T_e	T_m ice	Salinity
HH-1	Amygdule	Dolomite	P	L, L+V	62–89	–36/–45	n.d.	–1.5/–1.9	2.6–3.2
		Calcite	P	L, rarely L+V	n.d.	–36/–45	–37	–1.2/–1.9	2.1–3.2
HH-2	Amygdule	Quartz	P	L+V, L	56–>250	–37/–43	–34/–38	–0.3/–2.2	0.5–3.7
		Calcite II	P	L, rarely L+V	n.d.	–45	n.d.	–0.2	0.4
		Dolomite	P	L		–36/–42	n.d.	–0.1/–1.2	0.2–2.1
HH-3	Amygdule	Dolomite I	P	L+V	106–131	–37/–46	–35	–0.4/–1.0	0.7–1.7
		Dol. II+magn	P	L+V, L	143–151	–39/–44	n.d.	–1.1/–2.1	1.9–3.5
		Dolomite III	P	L+V, L	60–125	–37/–44	–37	–0.3/–1.5	0.5–2.6
			PS–S?	L, L+V	60–110	–35/–41	n.d.	–0.5/–1.2	0.9–2.1
HH-7	Vein	Calcite	P, PS	L, L+V	56–88	–35/–44	–34/–37	–0.2/–1.4	0.4–2.4
HH-17	Amygdule	Calcite	P	L+V, L	110–125	–34/–43	n.d.	–0.8/–1.2	1.4–2.1
PG	Amygdule	Fluorite	P, PS	L+V, rarely L	118–172	–30/–45	n.d.	–0.2/–0.6	0.4–1.1
			S	L, rarely L+V	48	–41	n.d.	–0.1	0.2

grained carbonate matrix (sample PG, leg. P. Gadas). Fluorite grains up to 1 cm in diameter are colourless, white and light violet in colour.

Fluid inclusions

Fluid inclusions suitable for microthermometric analysis were found in quartz, fluorite and carbonate from both vein and amygdule mineralizations (Table 3).

Carbonate (calcite, dolomite) samples contain abundant primary fluid inclusions, which are often concentrated within certain growth zones, whereas other zones are essentially inclusion-free. Such a distribution of fluid inclusions is typical especially for small dolomite amygdules in the sample HH-1, and the early dolomite I in sample HH-3. Primary fluid inclusions in some other samples (fluorite, dolomite III in sample HH-3) exhibit a regular three-dimensional distribution without apparent arrangement along growth zones.

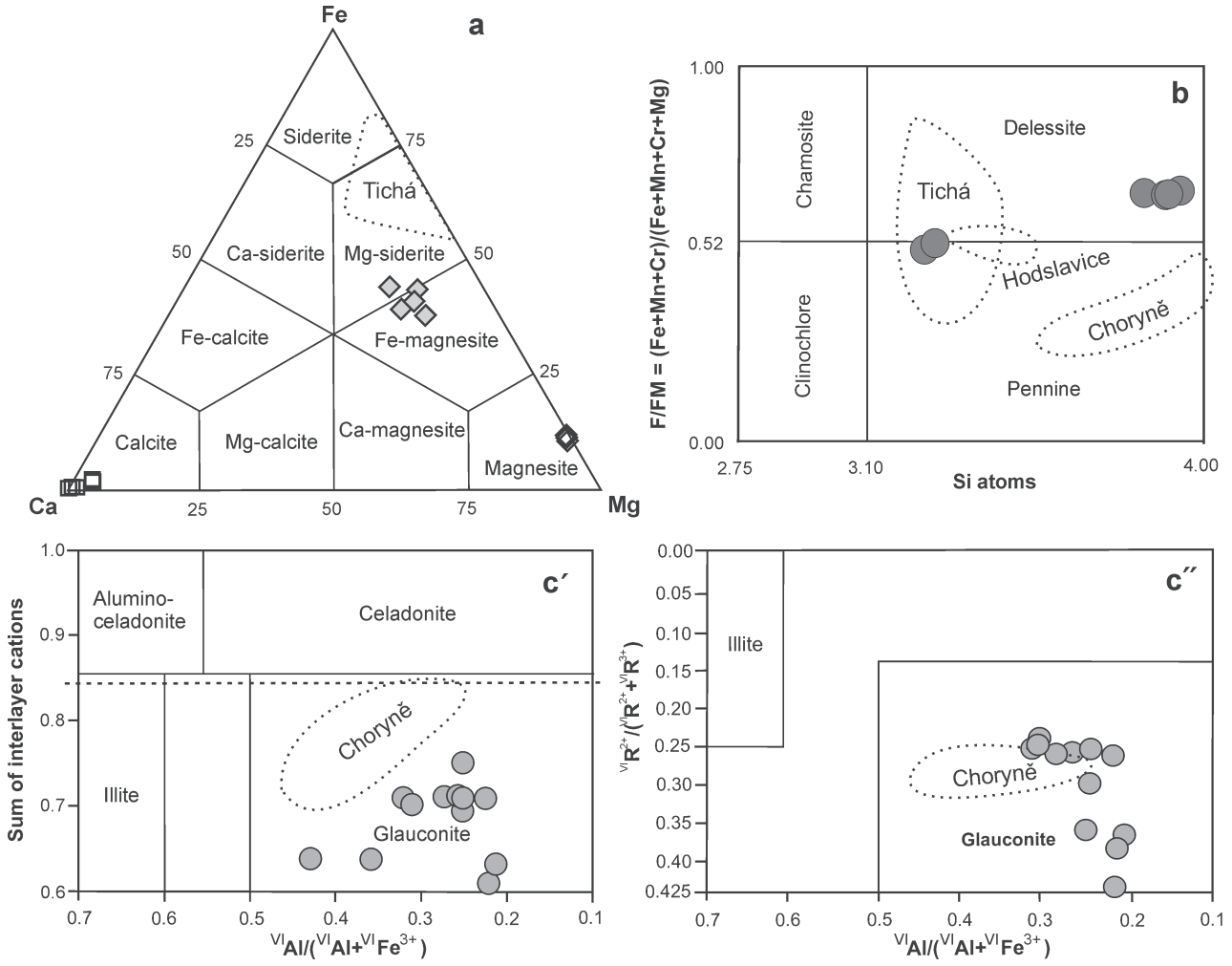

Fig. 3. Classification of some hydrothermal phases from Hončova hůrka and comparison with other teschenite/picrite hosted mineralizations. **a** — Carbonates of calcite group (Trdlička & Hoffman 1975). **b** — Chlorites (Melka 1965). **c** — Glauconite (Rieder et al. 1998). Figure **c′** represents the lateral view on 3D diagram, figure **c″** is top view along the cutting plane which is marked by dashed line in figure c′. The comparative data (outlined by dotted line) are from Urubek & Dolníček (2008), Urubek et al. (2009) and Dolníček et al. (2010).

Quartz HH-2 contains irregular clusters of fluid inclusions, which are situated mostly around the centre of the crystal, whereas the rims are essentially inclusion-free. Very rare solitary fluid inclusions have been observed in fine-grained dolomite II + magnesite mixture in sample HH-3 as well as in late calcite crystal in sample HH-2.

Most primary inclusions show equant shapes and sizes ranging between 5 and 26 μm. All samples contain aqueous inclusions only. At room temperature, a coexistence of one-phase (L-only) and two-phase (L + V) inclusions with essentially constant liquid-vapour ratios can be observed in most samples (the volume of gaseous phase does not exceed ca. 5 %). Both types of fluid inclusions occur together within the same structures (clusters, growth zones, etc.), however, the abundance of both compositional types varies significantly between samples (Table 3). The absence of vapour bubbles is often observed in smaller (< 10 μm) inclusions implying that metastability of the bubble nucleation could play a role. Few samples contain exclusively the L-only inclusions including those of larger sizes (e.g. calcite HH-2, dolomite HH-2) suggesting very low trapping temperatures (below ca. 50 °C; Goldstein & Reynolds 1994). Irregularly shaped inclusions in quartz HH-2 exhibit a wider variability in liquid-vapour ratios (up to ~30 % of vapour phase), possibly caused by necking-down.

Homogenization temperatures of primary L + V inclusions in carbonates and fluorite range between 56 and 172 °C (Fig. 4a). Quartz HH-2 alone exhibit even wider spread between 56 and >250 °C consistent with necked nature of fluid inclusions. In all samples, the inclusions freeze at temperatures from –34 to –45 °C. The vapour bubble was often eliminated by expanding ice, and during subsequent heating a metastable ice melting is common. In such cases, the fluid inclusions have been artificially stretched by overheating to ~200–250 °C prior to cryometric runs. The rarely observed eutectic temperatures are from –35 to –38 °C, suggesting the $NaCl\text{-}MgCl_2\text{-}H_2O$ fluid composition. The last ice melts at temperatures between –0.2 and –2.2 °C (Fig. 4b) indicating bulk fluid salinities between 0.4 and 3.7 wt. % NaCl eq. (Bodnar 1993). There are no systematic differences between L-only and L + V fluid inclusions in their cryometric

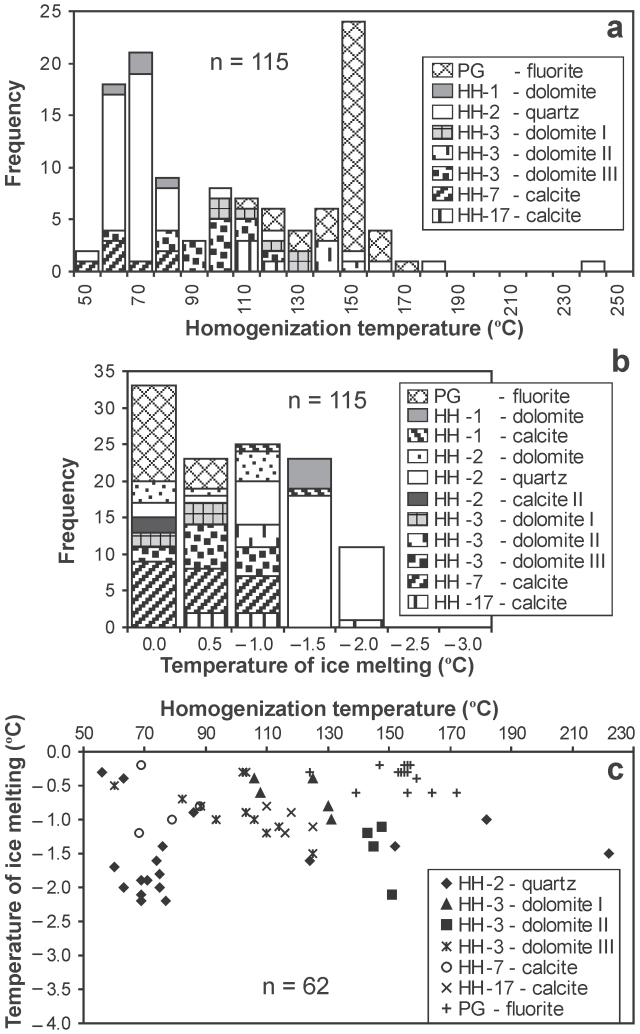

Fig. 4. Results of microthermometry of primary and primary-secondary fluid inclusions from Hončova hůrka. **a** — Histogram of homogenization temperatures of L+V inclusions. **b** — Histogram of temperatures of last ice melting. **c** — T_h–$T_m$ice plot. n — number of measurements.

parameters, which support the idea about a metastable nature of the liquid inclusions.

The irregularly-shaped secondary fluid inclusions arranged along healed microfractures are sometimes present in studied samples. They have generally similar microthermometric parameters as the primary fluid inclusions (Table 3).

C, O, S and Sr isotopes

Eight samples of carbonates were analysed for carbon and oxygen isotope compositions (Table 4). The $\delta^{18}O$ values vary between –0.6 and –6.5 ‰ PDB, and the $\delta^{13}C$ values are between –4.5 and +1.6 ‰ PDB.

One sample of sulphide sulphur, extracted from bulk amygdule HH-3, showed the $\delta^{34}S$ value as high as +1.1 ‰ CDT. Two attempts to collect a sufficient quantity of sulphur compounds for isotope analysis from host rocks were not successful.

The $^{87}Sr/^{86}Sr$ ratios were determined in five carbonate samples and two host rocks (Table 5). The lowest present-day $^{87}Sr/^{86}Sr$ ratios show both picrite samples (0.7045 and 0.7048 for the least and the most altered sample, respectively). All the hydrothermal carbonates exhibit considerably higher $^{87}Sr/^{86}Sr$ ratios between 0.7060 and 0.7068. The low values characterize the samples from picrite host rocks, the highest one originated from a vein calcite hosted by claystone.

Trace elements

Five carbonate separates and two samples of host picrite have been analysed for trace elements (Table 6). Low contents of elements incompatible with calcite structure (e.g. Ga, Zr, Rb) indicate a negligible contamination of carbonates by the host rock and/or hydrothermal silicate mineral phases. Low contents of heavy metals (except for Ni), low to moderate contents of Ba (32–515 ppm) and moderate to high contents of Sr (400–3700 ppm) were found in calcite and dolomite samples. The Ni content is elevated in all picrite-hosted samples (between 23 and 86 ppm), whereas the claystone-hosted calcite contains only 1.5 ppm Ni.

The two host rock samples exhibit similar chondrite-normalized REE patterns although they differ in both degree of alteration and total REE concentrations (164 and 281 ppm for least altered and strongly altered picrite, respectively). Both samples show LREE-enriched patterns (La_N/Yb_N=20 and 34) without any Ce and Eu anomalies (Fig. 5). In contrast, data on hydrothermal carbonates can be divided into two subsets differing in both absolute amount of REE and shape of normalized REE patterns. Group 1 is characterized by high content of REE (68–216 ppm) and LREE enrichment, which are both comparable to those of host picrite. The Ce and Eu anomalies are missing. Group 2 contains samples showing very low REE contents (0.12–0.93 ppm), with many elements below detection limit. The chondrite-normalized patterns are much more well-balanced in terms of LREE/HREE ratio (Fig. 5). No positive Eu anomalies are present but two of three samples exhibit a negative Ce anomaly (Ce/Ce*=0.68 and 0.72).

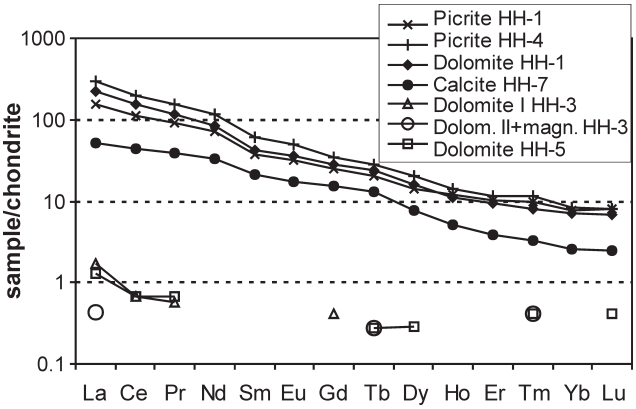

Fig. 5. REE chondrite-normalized patterns of hydrothermal carbonates and host picrite. Normalization values are from Anders & Grevesse (1989).

Table 4: Carbon and oxygen isotope composition of carbonates and $\delta^{13}C$ and $\delta^{18}O$ values of their parent fluids calculated for the given temperature.

Sample	Sample type	Mineral	$\delta^{13}C$ carb. (‰ PDB)	$\delta^{18}O$ carb. (‰ PDB)	$\delta^{18}O$ carb. (‰ SMOW)	Temperature (°C)	$\delta^{13}C$ fluid (‰ PDB)	$\delta^{18}O$ fluid (‰ SMOW)
HH-1	Amygdule	Dolomite	–3.7	–1.4	29.4	62–89	–6.1/–6.8	+2.9/+7.0
HH-2	Amygdule	Dolomite	–2.2	–0.6	30.3	30–50	–5.8/–7.0	–2.6/+1.6
		Calcite II	–4.5	–5.8	24.9	30–50	–7.9/–9.1	–2.0/+1.7
HH-3	Amygdule	Dolomite I	–3.4	–0.6	30.3	106–131	–5.6/–6.5	+10.0/+12.7
		Dol. II+magn	+1.6	–0.7	30.2	143–151	–0.5/–0.9	+13.7/+14.4
		Dolomite III	–3.8	–0.8	30.1	60–125	–5.9/–6.9	+3.2/+11.9
HH-5	Vein	Dolomite	–0.6	–5.0	25.7	n.d.	n.d.	n.d.
HH-7	Vein	Calcite	–3.5	–6.5	24.2	56–88	–5.7/–6.6	+1.9/+6.3

Table 5: Rb–Sr elemental and isotope data on samples from Hončova hůrka and calculated initial $^{87}Sr/^{86}Sr_i$ ratios for age of 120 Ma. The Rb contents in parentheses represent the maximum possible value, for which the initial $^{87}Sr/^{86}Sr_i$ ratio was calculated.

Sample	Sample type	Mineral	Rb (ppm)	Sr (ppm)	$^{87}Sr/^{86}Sr_m$	$\pm 2\sigma$	$^{87}Sr/^{86}Sr_i$
HH-1	Amygdule	Dolomite	1.0	1590	0.706586	0.000017	0.706583
HH-3	Amygdule	Dolomite I	(0.4)	400	0.706521	0.000020	0.706516
		Dol. II+magn	(0.4)	3700	0.706000	0.000018	0.705999
HH-5	Vein	Dolomite	(0.4)	800	0.705968	0.000019	0.705966
HH-7	Vein	Calcite	(0.4)	3390	0.706806	0.000019	0.706805
HH-1	Host rock	Picrite	34.7	900	0.704780	0.000019	0.704590
HH-4	Host rock	Picrite	34.4	510	0.704503	0.000018	0.704170

Table 6: Trace element abundances in carbonate and picrite samples from Hončova hůrka. All values are in ppm. The contents of Ag, As, Au, Be, Bi, Cd, Cs, Hg, Sb, Se, Sn, Tl and W in all samples were below or just around the detection limits ranging between 0.1 and 1 ppm.

Sample Mineral Sample type	HH-4 Picrite Host rock	HH-1 Picrite Host rock	HH-1 Dolomite Amygdule	HH-3 Dolomite I Amygdule	HH-3 Dol. II+magn Amygdule	HH-5 Dolomite Vein	HH-7 Calcite Vein
Ba	606	1150	515	262	86.9	74.7	32.1
Co	95.6	50.7	66.7	1.4	4.1	0.5	<0.5
Cu	37.8	50.1	16.7	0.5	0.1	0.2	0.4
Ga	18.9	13.6	<0.5	<0.5	<0.5	<0.5	<0.5
Hf	3.7	4.4	<0.5	<0.5	<0.5	<0.5	<0.5
Mo	1.9	0.2	<0.1	0.5	0.2	0.8	<0.1
Nb	61.9	86.6	<0.5	<0.5	<0.5	<0.5	<0.5
Ni	616	307	49.0	22.9	86.2	24.0	1.5
Pb	1.8	1.5	1.4	0.1	<0.1	0.6	0.7
Rb	34.4	34.7	1.0	<0.5	<0.5	<0.5	<0.5
Sc	19	28	n.d.	n.d.	n.d.	n.d.	n.d.
Sr	510	900	1590	400	3700	800	3390
Ta	3.2	4.7	<0.1	<0.1	<0.1	<0.1	<0.1
Th	4.2	9.2	0.9	<0.1	0.1	<0.1	0.2
U	1.8	2.3	0.8	1.9	1.4	0.3	<0.1
V	200	250	39	7	16	6	<5
Zn	72	51	45	3	7	4	<1
Zr	154	174	1.9	7.9	6.3	1.5	<0.5
Y	18.3	22.6	20.2	0.1	0.3	0.4	10.4
La	36.3	70.3	52.9	0.4	0.1	0.3	12.4
Ce	66.7	117	91.9	0.4	<0.1	0.4	26.6
Pr	8.15	13.71	10.34	0.05	<0.02	0.06	3.44
Nd	32.0	51.7	38.2	<0.3	<0.3	<0.3	15.0
Sm	5.59	8.78	6.23	<0.05	<0.05	<0.05	3.12
Eu	1.81	2.76	2.05	<0.02	<0.02	<0.02	0.98
Gd	4.86	6.76	5.64	0.08	<0.05	<0.05	3.03
Tb	0.72	1.00	0.86	<0.01	0.01	0.01	0.46
Dy	3.45	4.90	3.86	<0.05	<0.05	0.07	1.88
Ho	0.66	0.78	0.61	<0.02	<0.02	<0.02	0.29
Er	1.60	1.85	1.50	<0.03	<0.03	<0.03	0.61
Tm	0.24	0.28	0.19	<0.01	0.01	0.01	0.08
Yb	1.27	1.38	1.17	<0.05	<0.05	<0.05	0.42
Lu	0.19	0.19	0.16	<0.01	<0.01	0.01	0.06
Σ REE	164	281	216	0.93	0.12	0.86	68.4
La_N/Yb_N	19.8	35.3	31.4	n.d.	n.d.	n.d.	20.5
Ce/Ce*	0.93	0.90	0.94	0.68	n.d.	0.72	0.98
Eu/Eu*	1.06	1.09	1.05	n.d.	n.d.	n.d.	0.97

Discussion

Source of hydrothermal fluids

The available geochemical data offer several lines of evidence that the major source of parent hydrothermal fluids was not related to the host picrite:

Salinity of hydrothermal fluid. It is well documented that silicic magma can exsolve hydrosaline fluid phase during crystallization (e.g. Burnham 1979; Cline & Bodnar 1991; Webster 2004). The actual fluid salinity depends on (i) pressure (i.e. depth of intrusion) and (ii) progress in magmatic crystallization (Cline & Bodnar 1991; Fall et al. 2007). At pressures about 0.5 kbars (i.e. in shallow settings), the salinity of the earliest magmatic fluid is low and it increases rapidly during crystallization. At pressures about 1.3 kbars the salinity shows only minor changes towards higher values at the end of crystallization. In deep (pressures higher than ca. 2 kbars) systems the first fluid exsolved from the melt has high salinity and salinity decreases as crystallization proceeds. If the fluids at Hončova hůrka were magmatic in origin, then the observed occurrence of low-salinity solutions (that have to operate during the final stage of magmatic crystallization) would indicate the deep-seated high-pressure conditions (in depth at least 20 km under hydrostatic conditions). However, the occurrence of carbonate-rich sediments in the surroundings of the picrite body indicates that the seafloor was situated well above CCD at Hončova hůrka site (~4–5 km at maximum, cf. van Andel Tjeerd 1975 in Kiss et al. 2008). Thus the magmatic model alone is incompatible with observed data and geological situation, and alternative fluid source(s) must have been involved. Mixing of two fluid endmembers which differ in temperature and salinity can be inferred from the T_h-$T_m$ice diagram for all carbonate samples (Fig. 4c). The higher-salinity fluid endmember could possibly be seawater as is indicated from salinity reaching up to ~3.5 wt. % and the Na-Mg-Cl salt composition. The origin of the low-salinity fluid endmember cannot be specified from salinity data alone, but meteoric water as the usually most available source could be safely rejected in our submarine setting.

$\delta^{18}O$ and $\delta^{13}C$ of the hydrothermal fluid. The fluid $\delta^{18}O$ and $\delta^{13}C$ characteristics have been calculated from mineral $\delta^{18}O$ and $\delta^{13}C$ data using the measured homogenization temperatures or estimated crystallization temperatures (Table 4). It should be noted that the use of pressure-uncorrected T_h values leads to underestimated fluid $\delta^{18}O$ and $\delta^{13}C$ values. Fortunately the low-pressure systems need only insignificant correction. At Hončova hůrka the pressure does not exceed 500 bars (= depth of 5 km under hydrostatic conditions). A more detailed quantification is not possible from the available data. If the pressure attained the maximum value of 500 bars, then the measured T_h values need to be shifted by 15–25 °C to obtain real trapping temperatures (Flincor software; Brown 1989). Such an increase of temperature shifts both the fluid $\delta^{18}O$ and $\delta^{13}C$ values by 2.0–2.5 and 0.5–1.5 ‰, respectively. These (maximum possible) shifts do not affect the interpretation of carbon and water sources indicated below.

The fluid $\delta^{18}O$ values are widely scattered between ~0 and ~+14 ‰ SMOW overlapping significantly the range of magmatic waters (+5 to +10 ‰ SMOW; Sheppard 1986). The observed variability of $\delta^{18}O$ values could be explained by 1) highly variable exchange of oxygen between rocks and fluid phase, or 2) mixing of two (or more) fluids with contrasting isotope compositions (e.g. seawater with a near-zero $\delta^{18}O$ value could mix with metamorphic, diagenetic or organic waters with highly positive $\delta^{18}O$ values; cf. Sheppard 1986). In the given geological setting the generation of "diagenetic" low-salinity waters has been documented in clay-rich sedimentary sequences (cf. Polách et al. 2008; Dolníček & Polách 2009). The dewatering of clays could have been associated with burial compaction and/or heating-up caused by intrusion of teschenite/picrite magma.

Most samples show a limited range of calculated fluid $\delta^{13}C$ values (–6 to –9 ‰ PDB; Table 4) which largely overlap the values typical of "magmatic" carbon (–5 to –8 ‰ PDB; Hoefs 1997). However, the same range exhibits also "carbon of the homogenized Earth's crust", averaged from various crustal sources during fluid evolution. Nevertheless the influence of external sources is manifested by near-zero fluid $\delta^{13}C$ value of dolomite II from sample HH-3 indicating the source of carbon in sedimentary carbonates (limestones).

REE signature of hydrothermal fluid. The REE data on hydrothermal carbonates cluster in two internally consistent groups. Such a behaviour does not favour the interpretation in terms of crystallization from a single fluid enriched in REE-complexing ligands, where a continuous change in REE patterns of precipitating carbonates can be expected during crystallization. Rather, our data could reflect different sources of REE in the hydrothermal fluids and/or interaction with different rocks. While Group 1 samples could have been inferred from host picrite, Group 2 shows REE concentrations and patterns typical of Cretaceous marine limestones (Bellanca et al. 1997; Temur et al. 2009). The negative Ce anomaly in Group 2 samples could reflect the presence of seawater in the hydrothermal system (McLennan 1989); or a signature inherited from limestones.

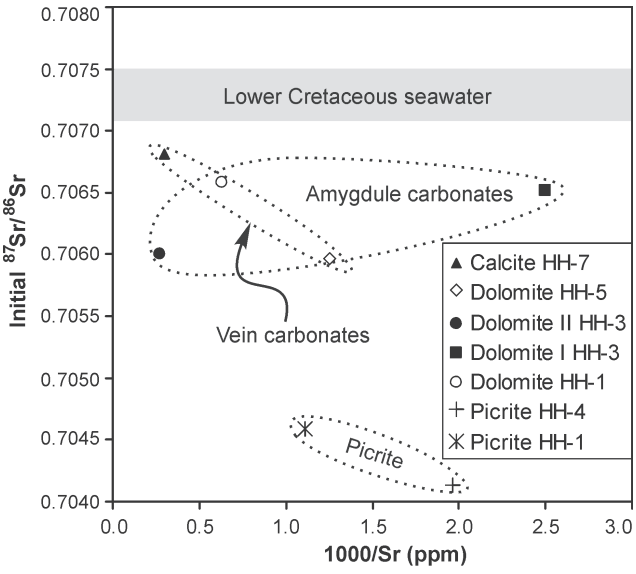

Fig. 6. $^{87}Sr/^{86}Sr_i$ vs. 1000/Sr plot for carbonate and picrite samples from Hončova hůrka.

Sr isotope composition of hydrothermal fluid. Table 5 gives the "initial" $^{87}Sr/^{86}Sr_i$ ratios calculated for age of 120 Ma. This age represents the solidification age of host igneous rock, and the uppermost possible age of the studied mineralization. Due to extremely low Rb/Sr ratios, the $^{87}Sr/^{86}Sr_i$ ratios of the carbonate samples are (within the analytical uncertainty) indistinguishable from the present-day $^{87}Sr/^{86}Sr$ values. The $^{87}Sr/^{86}Sr_i$ ratios of all hydrothermal carbonates are much higher (0.7060 to 0.7068) then those of host picrite (0.7042 and 0.7046) thus indicating an external source of at least a part of the strontium in the hydrothermal fluid. The possible sources of more radiogenic strontium are (i) Lower Cretaceous seawater ($^{87}Sr/^{86}Sr = 0.7071$ to 0.7075; Veizer et al. 1999), (ii) marine limestones occurring in rock sequences of the Silesian Unit, and/or (iii) siliciclastic sedimentary rocks. The probable influence of more then two sources of strontium is indicated by a lack of correlation between $^{87}Sr/^{86}Sr$ and 1000/Sr (Fig. 6).

Evidence for interaction with host picrite

As indicated above, many mineral-forming elements and major part of fluid phase have been derived out of the picrite body. However, the picrite body served not only as a suitable conduit for fluid flow and site for the associated precipitation of mineral phases, but there is evidence that the igneous rock has also actively interacted with hydrothermal fluids.

Picrite alteration and the nature of hydrothermal mineralization. The nature and mineral composition of secondary phases in host picrite are similar to those in the studied amygdule and vein parageneses: in both cases phyllosilicates and carbonates predominate. Therefore, it is probable that pervasive alteration of picrite was coeval with hydrothermal activity giving rise to the open-space mineralization (cf. Kudělásková et al. 1990). Two specific features can further support this opinion. 1) The vein and amygdule mineralization is characterized by a pronounced enrichment in magnesium. The iron-poor dolomite as a dominating gangue mineral as well as the presence of magnesite is not known from other sites in the sub-Beskydy magmatic province. The occurrence of these phases is coupled with an increase of FeO/(FeO + MgO) ratio from 0.35 to 0.43 during increasing intensity of picrite alteration (Table 1) implying that magnesium was preferentially leached from the rock by circulating fluids. 2) The mineralization at Hončova hůrka contains elevated contents of Ni in pyrite and carbonates. In addition, a trace amount of millerite is described for the first time here. The Ni-enrichment of the fluid phase is coupled with Ni-depletion of altered rocks (Table 6), again suggesting a source of this element in the host rock (olivine in the sample HH-4 contains up to 0.23 wt. % NiO; unpubl. microprobe data of the authors). Both the above mentioned findings are unique for the Hončova hůrka site only. This can evoke an idea about low water-rock ratio during alteration/mineralization process in order to allow the increasing Mg and Ni concentration in the fluid to the level at which the Mg- and Ni-rich phases can precipitate. However the available data on fluid salinity and REE fractionation from Hončova hůrka are comparable to those from other (teschenite/picrite-hosted and dolomite-magnesite-millerite free) mineralizations (cf. Polách 2008; Urubek 2009) suggesting that hydration reactions did not shift the contents of both salts and strong REE-complexing ligands in the remaining fluid phase. This behaviour would favour the open-system fluid circulation and higher water-rock ratios (cf. Dolníček et al. 2010; Kiss et al. 2008).

$\delta^{34}S$ of the hydrothermal fluid. The near-zero $\delta^{34}S$ value of fluid-precipitated sulphides is compatible with mantle-derived sulphur (Hoefs 1997), which could have been leached from the host picrite. However, it must be noted that such a $\delta^{34}S$ value can also be generated by a variety of other processes.

Conclusion

The vein and amygdule mineral assemblages hosted by a submarine effusive body of Lower Cretaceous picrite at Hončova hůrka Hill exhibit largely similar fluid inclusion and geochemical parameters although they can differ significantly in mineral compositions and texture. This suggests that they are related to the same mineralizing event. Besides the dominating dolomite, magnesite, siderite, quartz, calcite, chlorite, glauconite, fluorite, barite, pyrite and millerite were also identified. The parent fluids are characterized by variable but generally low temperatures (< 50–170 °C), low salinities (0.4 to 3.7 wt. %), low content of strong REE-complexing ligands, near-zero to highly positive (up to + 14 ‰ SMOW) $\delta^{18}O$ values, near-zero to negative (down to –9 ‰ PDB) $\delta^{13}C$ values, near-zero $\delta^{34}S$ value, and initial $^{87}Sr/^{86}Sr$ ratios much more radiogenic (0.7060 to 0.7068) than those of the host picrite (0.7042 and 0.7046). These data are inconsistent with an orthomagmatic picrite-related origin of the parent fluids, which are interpreted to be predominantly of external origin derived by mixing of seawater with diagenetic waters, the latter produced by dewatering of clay minerals in associated flysch sediments. The isotope and REE signatures indicate interaction of at least a part of the fluids with sedimentary carbonates prior to mineral precipitation. The interaction of the fluids with the host picrite led to strong alteration of the rock and leaching of some elements (Mg, Ni, S, partly also REE) that participated later during precipitation of vein- and amygdule-hosted hydrothermal phases.

Acknowledgments: The study was supported by Project GAČR 205/07/P130. M. Dosbaba and P. Gadas (MU Brno) are thanked for assistance during microprobe work. Special thank is to P. Gadas for providing the fluorite sample. The isotope analyses conducted by I. Jačková, Z. Lněničková, V. Janoušek and V. Erban (ČGS Praha) are highly appreciated. Constructive comments by three journal reviewers (V. Hurai, F. Molnár and an anonymous one) helped to improve the initial draft of the manuscript.

References

Anders E. & Grevesse N. 1989: Abundances of the elements: Meteoritic and solar. *Geochim. Cosmochim. Acta* 53, 197–214.

Bellanca A., Masetti D. & Neri R. 1997: Rare earth elements in limestone/marlstone couplets from the Albian-Cenomanian Cismon

section (Venetian region, northern Italy): assessing REE sensitivity to environmental changes. *Chem. Geol.* 141, 141–152.

Bernard J.H., Čech F., Dávidová Š., Dudek A., Fediuk F., Hovorka D., Kettner R., Koděra M., Kopecký L., Němec D., Paděra K., Petránek J., Sekanina J., Staněk J. & Šímová M. 1981: Mineralogy of the Czechoslovakia. *Academia,* Praha, 1–615 (in Czech).

Bodnar R.J. 1993: Revised equation and table for determining the freezing point depression of H_2O-NaCl solutions. *Geochim. Cosmochim. Acta* 57, 683–684.

Brown Ph.E. 1989: FLINCOR: A fluid inclusion data reduction and exploration program. *Second biennial Pan-American conference on research on fluid inclusions, program with abstracts*, 14.

Burnham C.W. 1979: Magmas and hydrothermal fluids. In: Barnes H.L. (Ed.): Geochemistry of hydrothermal ore deposits. 2nd ed. *J. Wiley and Sons*, New York, 71–136.

Cline J.S. & Bodnar R.J. 1991: Can economic porphyry copper mineralization be generated by typical calc-alkaline melt? *J. Geophys. Res.* 96, 8118–8126.

Dolníček Z. & Polách M. 2009: Hydrothermal mineralization in sandstones of Variegated Godula Member at the locality Bystrý potok (Moravskoslezské Beskydy Mts.). *Acta Mus. Moraviae, Sci. Geol.* 94, 97–110 (in Czech).

Dolníček Z., Kropáč K., Uher P. & Polách M. 2010 online: Mineralogical and geochemical evidence for multistage origin of mineral veins hosted by teschenites at Tichá, Outer Western Carpathians, Czech Republic. *Chem. Erde.* doi: 10.1016/j.chemer.2010.03.003

Dostal J. & Owen J.V. 1998: Cretaceous alkaline lamprophyres from northeastern Czech Republic: geochemistry and petrogenesis. *Geol. Rdsch.* 87, 67–77.

Eliáš M. 1970: Lithology and sedimentology of the Silesian Unit in the Moravskoslezské Beskydy Mts. *Sborn. Geol. Věd, Geol.* 18, 7–99 (in Czech).

Fall A., Bodnar R.J., Szabó Cs. & Pál-Molnár E. 2007: Fluid evolution in the nepheline syenites of the Ditrău Alkaline Massif, Transylvania, Romania. *Lithos* 95, 331–345.

Goldstein R.H. & Reynolds T.J. 1994: Systematics of fluid inclusions in diagenetic minerals. *Soc. Sed. Geol., Short Course* 31, 1–199.

Grabowski J., Krzeminski L., Nescieruk P., Szydlo A., Paszkowski M., Pécskay Z. & Wójtowicz A. 2003: Geochronology of teschenitic intrusions in the Outer Western Carpathians of Poland — constraints from $^{40}K/^{40}Ar$ ages and biostratigraphy. *Geol. Carpathica* 54, 385–393.

Hoefs J. 1997: Stable isotope geochemistry. 4th ed. *Springer Verlag*, Berlin, New York, 1–244.

Hovorka D. & Spišiak J. 1988: Mesozoic volcanism in the Western Carpathians. *Veda*, Bratislava, 1–263 (in Slovak).

Jarchovský J. 1960: Analysis of silicate rocks. *SVTL*, Bratislava, 1–238 (in Slovak).

Kiss G., Molnár F. & Palinkas L.A. 2008: Volcanic facies and hydrothermal processes in Triassic pillow basalts from the Darnó Unit, NE-Hungary. *Geol. Croatica* 61, 2–3, 385–394.

Kudělásková J. 1987: Petrology and geochemistry of selected rock types of teschenite association, Outer Western Carpathians. *Geol. Carpathica* 38, 545–573.

Kudělásková J., Kudělásek V. & Matýsek D. 1990: Zeolites in picrite of the teschenite association at the locality Hončova Hůrka near Příbor (Northern Moravia). *Čas. Mineral. Geol.* 35, 317–321 (in Czech).

Lucińska-Anczkiewicz A., Villa I.M., Anczkiewicz R. & Ślaczka A. 2002: $^{40}Ar/^{39}Ar$ dating of alkaline lamprophyres from the Polish Western Carpathians. *Geol. Carpathica* 53, 45–52.

Matsuhisa Y., Morishita Y. & Sato T. 1985: Oxygen and carbon isotope variations in gold-bearing hydrothermal veins in the Kushikino mining area, southern Kyushu, Japan. *Econ. Geol.* 80, 283–293.

Matýsek D. 1989: Geochemical classification of rock of teschenite association. *Sborn. Věd. Prací Vys. Šk. Báň. Ostr.* 35, 301–324 (in Czech).

McCrea J.M. 1950: On the isotopic chemistry of carbonates and a palaeotemperature scale. *J. Chem. Phys.* 18, 849–857.

McLennan S.M. 1989: Rare earth elements in sedimentary rocks: influence of provenance and sedimentary processes. *Rev. in Mineralogy* 21, 169–200.

Melka K. 1965: A proposal of classification of chlorite minerals. *Věst. Ústř. Úst. Geol.* 40, 23–27 (in Czech).

Narębski W. 1990: Early rift stage in the evolution of western part of the Carpathians: geochemical evidence from limburgite and teschenite rock series. *Geol. Carpathica* 41, 521–528.

Ohmoto H. & Goldhaber M.B. 1997: Sulfur and carbon isotopes. In: Barnes H.L. (Ed.): Geochemistry of hydrothermal ore deposits. 3rd ed. *J. Wiley & Sons*, New York, 517–611.

O'Neil J.R., Clayton R.N. & Mayeda T.K. 1969: Oxygen isotope fractionation in divalent metal carbonates. *J. Chem. Phys.* 51, 5547–5558.

Pacák O. 1926: Volcanic rocks at the northern footwall of the Moravské Beskydy Mts. *Rozpr. Českosl. Akad. Věd Umění* 35 (in Czech).

Plašienka D., Grecula P., Putiš M., Kováč M. & Hovorka D. 1997: Evolution and structure of the Western Carpathians: an overview. In: Grecula P., Hovorka D. & Putiš M. (Eds.): Geological evolution of the Western Carpathians. *Miner. Slovaca—Monograph*, Bratislava, 1–24.

Polách M. 2008: Hydrothermal mineralization in the eastern part of the Moravskoslezské Beskydy Mts. (Outer West Carpathians). *MSc. Thesis, UP Olomouc,* 1–74 (in Czech).

Polách M., Dolníček Z. & Malý K. 2008: Hydrothermal mineralization at the locality Pindula near Frenštát pod Radhoštěm (Silesian unit, Outer West Carpathians). *Acta Mus. Moraviae, Sci. Geol.* 93, 127–135 (in Czech).

Pouchou J. & Pichoir F. 1985: "PAP" procedure for improved quantitative microanalysis. *Microbeam Anal.* 20, 104–105.

Rieder M., Cavazzini G., D'Yakonov Y., Frank-Kamenetskii V.A., Gottardi G., Guggenheim S., Koval P.V., Müller G., Neiva A.M.R., Radoslovich E.W., Robert J.L., Sassi F.P., Takeda H., Weiss Z. & Wones D.R. 1998: Nomenclature of the micas. *Canad. Mineralogist* 36, 905–912.

Roedder E. 1984: Fluid inclusions. *Rev. in Mineralogy* 12, 1–644.

Rusek P. & Valošek Č. 1968: Hončova hůrka near Příbor — an interesting mineralogical locality. *Přírodověd. Sbor. k 60. výročí Přírodověd. společnosti v Ostravě* 24, 79–88 (in Czech).

Shepherd T.J., Rankin A.H. & Alderton D.H.M. 1985: A practical guide to fluid inclusion studies. *Blackie*, Glasgow and London, 1–239.

Sheppard S.M.F. 1986: Characterization and isotopic variations in natural waters. *Rev. in Mineralogist* 16, 165–183.

Smulikowski K. 1929: Les roches eruptives de la zone subbeskidique en Silesie et Moravie. *Kosmos B* 54, 749–850.

Spišiak J. & Hovorka D. 1997: Petrology of the Western Carpathians Cretaceous primitive alkaline volcanics. *Geol. Carpathica* 48, 113–121.

Steiger R.H. & Jäger E. 1977: Subcommission on geochronology: convention on the use of decay constants in geo- and cosmochronology. *Earth Planet. Sci. Lett.* 36, 359–362.

Sušeň P. 2000: The Petřkovická Hůrka Hill near Valašské Meziříčí. *Minerál* 8, 104–107 (in Czech).

Šmíd B. 1962: An overview of geology and petrography of rocks of teschenite association from the northern footwall of the Beskydy Mts. *Geol. Práce* 63, 53–60 (in Czech).

Temur S., Orhan H. & Deli A. 2009: Geochemistry of the limestone of Mortas Formation and related terra rossa, Seydisehir, Konya, Turkey. *Geochem. Int.* 47, 67–93.

Trdlička Z. & Hoffman V. 1975: Study of chemical composition of

vein carbonates from Kutná Hora (ČSSR). *Freiberg. Forschungshefte* 6, 29–81 (in Germany).

Trundová A. 2004: Petrology of teschenites from selected localities in the Moravskoslezské Beskydy Mts. *MSc. Thesis, MU Brno* (in Czech).

Ueda A. & Krouse H.R. 1987: Direct conversion of sulphide and sulphate minerals to SO_2 for isotope analyses. *Geochem. J.* 20, 209–212.

Urubek T. 2009: Hydrothermal mineralization in western part of the Silesian Unit (Outer Western Carpathians: genetic aspects. *MSc. Thesis, UP Olomouc*, 1–87 (in Czech).

Urubek T. & Dolníček Z. 2008: Hydrothermal mineralization in rocks of teschenite association from Hodslavice near Nový Jičín (Silesian unit, Outer West Carpathians). *Čas. Slez. Muz. Opava (A)* 57, 21–30 (in Czech).

Urubek T., Dolníček Z. & Uhlíř D. 2009: Mineralogy and formation conditions of the hydrothermal mineralization in picrite from Choryně near Valašské Meziříčí (Silesian Unit, Outer Western Carpathians). *Čas. Slez. Muz. Opava (A)* 58, 175–190 (in Czech).

Veizer J., Ala D., Azmy K., Bruckschen P., Buhl D., Bruhn F., Carden G.A.F., Diener A., Ebneth S., Godderis Y., Jasper T., Korte Ch., Pawellek F., Podlaha O.G. & Strauss H. 1999: $^{87}Sr/^{86}Sr$, $\delta^{13}C$ and $\delta^{18}O$ evolution of Phanerozoic seawater. *Chem. Geol.* 161, 59–88.

Webster J.D. 2004: The exsolution of magmatic hydrosaline chloride liquids. *Chem. Geol.* 210, 33–48.

Wlodyka R. & Karwowski L. 2004: The alkaline magmatism from the Polish Western Carpathians. *Pol. Tow. Miner., Pr. Spec.* 24, 23–31.